Proof-of-Concept Validation of Noninvasive Detection of Cortical Spreading Depolarization with High Resolution Direct Current-Electroencephalography

Benjamin R. Brown, PhD [1]
Samuel J. Hund, PhD [1,2]
Kirk A. Easley, MS, MApStat [3]
Eric L. Singer, MS [1]
C. William Shuttleworth, PhD [4]
Andrew P. Carlson, MD [5]
Stephen C. Jones, PhD [1]

[1] CerebroScope, the dba entity of SciencePlusPlease LLC, 4165 Blair St., Pittsburgh, PA 15207-1508, USA
[2] SimulationSolutions, LLC, 5707 Jackson St., Pittsburgh, PA, 15206, USA
[3] Department of Biostatistics and Bioinformatics, Rollins School of Public Health, Emory University, 1518 Clifton Road NE, Atlanta, GA, 30322, USA
[4] Department of Neurosciences, University of New Mexico School of Medicine, Albuquerque, NM, USA
[5] Department of Neurosurgery, University of New Mexico School of Medicine, Albuquerque, NM, USA

Correspondence to:
Stephen C. Jones, PhD
CerebroScope
412-208-3397
412-849-9584 (cell)
sjones0123@alum.mit.edu
sjones@cerebro-scope.com``

Number of text pages and words: Abstract 382 words, 23 pages total with Tables and Figures with Legends), 9 pages, 5997 words without abstract etc.
Number of figures and tables: One table, 3 figures

Running Head: Noninvasive detection of cortical spreading depolarization

Abstract

Background/Objective: Cortical spreading depolarization (SD) is increasingly recognized as a major contributor to secondary brain injury. Monitoring SDs could be used to institute and guide SD-based therapeutics if noninvasive detection methods were available. Our primary objective is to use a high density array of electrodes to compare scalp direct current (DC)-shifts to SDs detected by gold standard electrocorticography (ECoG) to establish proof-of-concept validation that scalp DC-potentials can potentially provide noninvasive SD detection. Our secondary objective is to assess usability and artifact tolerance.

Methods: An 83x58 mm thermoplastic elastomer array with 29 embedded 6-mm diameter Ag/AgCl 1-cm spaced electrodes, the CerebroPatch™ Proof-of-Concept Prototype, was adhesively placed on the forehead with an intervening electrode gel interface to record DC-electroencephalography in normal volunteers and severe acute brain injury patients in the neuro-intensive care unit some with and some without invasive subdural ECoG electrodes. The scalp and ECoG voltages were collected by a Moberg® Advanced ICU Amplifier. Artifacts were visually identified and usability issues were recorded. SD was scored on ECoG using standard criteria of DC shift with associated suppression of high frequency activity with propagation across the electrode. A six parameter Gaussian plus quadratic baseline model was used to produce time-course ECoG and scalp electrode channel plots and heat-map movies of scalp voltages. The similarity of the noninvasive scalp and invasive ECoG DC-shift time-courses was compared via the Gaussian fit parameters and confirmed if the Coefficient-of-Determination exceeded 0.80.

Results:

Usability and artifact issues obscured most scalp Prototype device data except for 38 of the 140 ECoG-coded SDs over a period of 11 days in one sub-arachnoid hemorrhage patient. 26 of these DC-shifts were in readable, artifact free portions of scalp recordings and 24 had an acceptable, >0.80 Coefficient-of-Determination (0.98 [0.02], median [IQR]) between invasive ECoG and noninvasive Prototype device DC-shifts. These data suggest that these scalp DC-shifts (peak -457 ± 69 μV [mean ± StD], full-width-half maximum 70.9 ± 5.92 sec, area 18.7 ± 2.76 cm^2) depicted in the heat-map movies represent noninvasively detected SDs.

Conclusions: These results suggest that noninvasive SD detection is possible using scalp DC-potential signals with a high spatial resolution EEG array. Efforts to limit artifact and improve usability in DC-EEG detection are needed in order to improve the reliability of this approach and enable multi-modal monitoring for secondary brain injury.

Keywords: Noninvasive Detection; DC-EEG, Cortical Spreading Depolarization; Electroencephalography; Electrocorticography; Secondary brain injury

Introduction

Cortical spreading depolarizations (SDs) are slowly travelling ~3-mm diameter regions of depolarized neurons and glial cells that travel as waves in the cerebral gray matter in which evoked and spontaneous electroencephalography (EEG) are suppressed [1-4]. This en masse depolarized region causes a negative swing in field potential of 5 to 30 mV [5, 6] that is reduced by ~90% at the scalp surface [6, 7]. In humans, SDs have been found to follow severe acute brain injuries (sABIs) [3, 4], including malignant hemispheric stroke, severe traumatic brain injury, and sub-arachnoid hemorrhage (SAH). SDs are also associated with migraine auras [4, 8, 9], concussion [7, 10, 11], and high-grade malignant glioma [12-14]. SDs spread at a rate of 1-9 mm/min across the cortical surface [1, 2, 15], thus taking tens of minutes to travel across the human brain surface.

The commonly used methods to detect SD in humans are invasive. These methods include the direct placement of electrocorticography (ECoG) electrode strips onto the cortical surface [16, 17] requiring either a craniotomy [18] or an enlarged burr hole [18, 19]. This invasive SD detection method is considered the gold standard with its three criteria as defined by the CoOperative Study on Brain Injury Depolarizations (COSBID) identification criteria that include a propagating DC-shift and its associated EEG suppression [20, 21]. Alternatively, depth electrodes can be used to detect SD either placed horizontally and subdurally in an extraventricular drainage burr hole [22, 23] or inserted intracortically via a multimodal monitoring bolt placed at the bedside [24, 25]. To answer the often expressed need for noninvasive SD detection [4, 20, 26] there have been several efforts directed at scalp SD detection: one attempt demonstrated scalp direct current (DC)-shifts and EEG suppression but not SD propagation so was partially successful [6]. Other efforts used decompressive craniotomy patients with a portion of their skulls removed that provided overly favorable conditions but showed some promise in such patients [27-29]. Another attempt using similar noninvasive methods but without ECoG was completely unsuccessful [30, 31]. Recently a case study reported retrospectively visually identified decreases in EEG delta band (0-4 Hz) power that were time-associated with depth electrode ECoG suppressions and DC shifts of a SD [32], suggesting another possible method of noninvasive SD detection. Another study demonstrated scalp EEG detection of SDs associated with epileptiform field potentials [33]. All three SD-identification aspects of the gold standard COSBID criteria [20, 21] were successfully recorded, but this study did not provide ground truth confirmation [33]. Of course, artifacts occur in all of these methods so must be addressed accordingly [34].

Simulation studies of both the primary DC-shift [7] and the secondary EEG suppression [35] attributes of SD have been used to better define effective methods for noninvasive detection. One simulation effort used silent cortical dipoles imbedded in a realistic brain model to simulate 0.5-40 Hz EEG suppression to explore the well-known variation in suppression duration and width as a determinant of detectability [35]. Hund et al. [7] used finite element analysis based on Poisson's equation to perform numerical simulations that estimated the scalp DC-potentials from a concussive brain surface SD modeled as an expanding ring. Hund et al. [7] then used these estimates of brain-surface DC-potential were then used to explore the optimal electrode configuration for reliable scalp SD detection and showed that closely-spaced electrodes are a necessary component for faithful noninvasive detection using DC-EEG. These simulation results [7, 35] suggest that the several centimeter electrode spacing for exploring noninvasive detection that was used in previous studies [6, 27] was not optimal and made noninvasive detection of SD difficult. Combining these distinctly different but complimentary simulation efforts [7, 35] might serve to advance noninvasive SD detection as both are markers of SD identification as defined by the invasive ECoG method [20, 21].

Secondary brain injury, SD, and SD-based Therapeutics

Secondary brain injury results in increased brain damage, increased mortality and morbidity, and more extensive rehabilitation during the 2-week extended period in the neuro-intensive care unit (ICU) following sABI [36, 37]. Evidence that SDs play a causal role in the pathogenic process of secondary brain injury and lead to progressive brain infarction [38] is supported by many clinical studies by the COSBID group. These studies show that SDs: 1) increase the area of necrosis [15, 18, 39-42]; 2) are

associated with unfavorable outcomes in severe traumatic brain injury [26, 41]; and 3) can be used to predict outcome and initiative rescue measures in aSAH [43]. Recently, the duration of SD-induced EEG suppression has been associated with infarct progression in malignant hemispheric stroke patients [44].

This evidence highlights the need for therapeutic interventions for secondary brain injury that target SD and, more importantly, for a noninvasive SD detection method to evaluate their effectiveness. Noninvasive SD monitoring could provide the possibility of full-scale testing in large clinical trials of successful small-scale pilot studies of SD-based therapies using ketamine [45], cilostazol [46], nimodipine [47], and other agents [48]. Other possible SD therapies include those currently being explored for the SD phase of migraine with aura [49-56]. The availability of noninvasive SD monitoring would add a direct measure of the presumptive primary cause of secondary brain injury to multi-modal monitoring stategies for existing [57, 58] and emerging [59-61] standards of care. The addition of noninvasive SD monitoring to the armamentarium for secondary brain injury might also augment the advances in improved outcome from stroke-specific treatment in the neuro-ICUs of certified stroke centers [62].

We present proof-of-concept validation data showing the close correspondence between ECoG-identified SDs and slow potential changes characterized by DC-shifts that occur over a period of about 3 minutes detected from the forehead-placed CerebroPatch™ Proof-Of-Concept Prototype (see Figure 1) as well as artifact and usability data to inform future device design. Our hypothesis is that DC-potentials recorded by closely-spaced scalp electrodes can be associated with ECoG-detected SDs and that these scalp DC-potentials provide noninvasive SD detection but that artifact and usability issues must be addressed in an improved electrode array design.

Methods

CerebroPatch™ Proof-of-Concept Prototype description

The CerebroPatch™ Proof-of-Concept Prototype electrode array (see Figure 1) is a single-layer 83x58 mm thermoplastic elastomer scaffold (Dynaflex™ G2706-1000-00, Avient Corporation, Avon Lake, OH) encasing a 1-cm spaced hexagonal array of 29 6-mm diameter 1.3-mm thick sintered Ag/AgCl electrodes (BMD-6, Biomed Products Inc., Fair Oaks, CA) with a 0.5 mm lip such that the active diameter is reduced to 5 mm. The array was fixed on the forehead with a double-sided adhesive membrane (3M 1522 Medical Double Coated Tape, 3M Corporation, Saint Paul, MN) cut to conform to the array outline and 5-mm electrode openings. Electrode gel (Ten20® Conductive Paste, Weaver and Company, Aurora, CO) filled the 1-mm space between the Ag/AgCl electrodes and the skin after the skin was prepped with Lemon Prep™ (Mavidon Corp., Flat Rock, NC) and cleaned with sterile water.

Human study issues

The CerebroPatch™ Proof-of-Concept Prototype was classed as Non-Significant Risk device during the protocol's evaluation and ethical approval by the Institutional Review Board of the University of New Mexico Human Research Protections Office (UNM HRPO 18-051). Informed consent was obtained from the participants or a legally authorized representative.

Protocol Details

This proof-of-concept study consisted of three cohorts with five subjects each: Cohort 1 consisted of normal subjects; Cohort 2 included neuro-ICU patients with ischemic stroke, intracranial hemorrhage, severe traumatic brain injury, or SAH who were implanted with a 1x6 ECoG strip electrode (AU1X6P Auragen 1x6 Cortical Strip Platinum, Integra LifeSciences Corporation, Plainsboro, NJ) placed at the time of craniotomy for their sABIs; and Cohort 3 were similar patients to Cohort 2 but with intact skulls. In Cohort 2 patients the CerebroPatch™ Proof-of-Concept Prototype device was placed on the forehead over the 6-electrode ECoG strip. No direct confirmation of their co-registration was possible as the Prototype device was removed for imaging procedures and every 24 hours to record a skin irritation score. It was then re-gelled and reapplied. The skin irritation score consisted of the sum of scores for erythema and edema reactions according to Table 1 in ISO 10993-10 [63]. In Cohort 3

patients the Prototype device was placed on the forehead over the presumed edge of the lesion. Cohort 1 participants were monitored for 2 hours. In Cohorts 2 and 3 monitoring was continued for up to 14 days.

Data collection, ECoG SD coding, and data analysis

Voltages from the CerebroPatch™ Proof-of-Concept Prototype and the ECoG strip were collected by a DC-coupled Moberg® CNS Advanced ICU Amplifier (Moberg Research Inc., Micromed Group, Ambler, PA) at 256 Hz. ECoG recordings were coded for SDs and isoelectric SDs (ISDs) using standard COSBID criteria [20, 21] by the study site principal investigator, APC, using LabChart software (ADInstruments, Inc., Colorado Springs CO, USA). Only times with valid ECoG recording were scored. Briefly, SDs were identified as a characteristic DC-potential shift coupled with suppression of clinical-frequency (0.5-50 Hz) ECoG data. Ideally these events also displayed propagation across the electrode. The duration of ECoG suppression was also recorded. If a characteristic DC-shift occurred in a period when the EEG signal was absent indicating isoelectric tissue, then it was coded as an ISD.

For further analysis, the brain-surface ECoG and scalp Prototype device signals were converted to EDF+ format [64] and processed using lab-designed Python scripts. The 256 Hz data was pre-processed in all 29 channels of the Prototype device and 6 channels of the ECoG strip by determining the mean voltage within non-overlapping eight second segments, reducing the signal sample rate to 0.125 Hz, consistent with oversampling by a factor of ~20 based on the estimated SD frequency of 0.006 Hz.

Detrended time-course channel plots of ECoG and CerebroPatch™ Proof-of-Concept Prototype voltages were generated after the data were segmented into overlapping 2-hr “brick-layer” epochs (to minimize edge effects from the detrending procedure). The detrending procedure consisted of fitting a 2 hr epoch to a linear function, and then subtracting this function from the data, to provide a linear baseline over the 2 hr data block. These data sets were then used to generate heat-map movies of the Prototype device data for visualization of the scalp electric field. This visualization involved interpolating the voltage between the sensors via Gaussian-based radial basis functions [65, 66] using a square grid with 0.33 mm spacing. A radial Gaussian profile of width equal to the sensor spacing (1 cm) was used without smoothing.

Readable portions of CerebroPatch™ Proof-of-Concept Prototype channel plots with minimal artifacts were visually assessed by SCJ. Recording periods were classed as unreadable based on the presence of any of the following:

1. Excessive and large amplitude artifacts with frequencies that obscured SDs;
2. DC-shifts that occurred in all Prototype device channels at the same time;
3. A high auto-scale range (above 1000 μV) indicative of artifacts; or
4. A low scale range (below 50 μV) indicative of a “no recording” period.

The scale range was chosen by excluding the most extreme 1% of the values to display just the middle 99% of the data.

Criteria of identifying scalp DC-shifts that are associated with ECoG-coded SDs

DC-shifts from the CerebroPatch™ Proof-of-Concept Prototype channel plots and heat-map movies were classed as acceptable for comparison with the ECoG DC-shifts from coded SDs using the following criteria 1, 2, and 3 and 4 if appropriate:

1. A DC-shift of varying amplitude occurred in more than one channel, but not all channels, as observed both in the movies and channel plots. For instance, Figure 2B shows the varying amplitude of channels B1 through B6 and the lack of signal in channels A1, C1, C2, and D3.
2. The magnitude of the DC-shifts were between -230 to -1200 μV. This is consistent with the range of 7% [7] and 12% [67] estimated and 3% experimental [7] scalp/brain-surface voltage ratios applied to the 1st and 3rd quartiles of ECoG amplitudes of -7.2 mV to -10.1 mV [7] as derived retrospectively from Drenckhahn et al.’s [6] data as reported by Hund et al. [7].
3. The spatial extent estimated from the DC-shift movies is ~4 cm to be consistent with the estimated x12 spatial spread of the ECoG DC-shifts [7, 67].

4. A DC-shift occurs repetitively in the same location. This repetition criteria is based on the COSBID criteria for identifying SDs from Dreier et al. [20; p.22; last paragraph: 'similar pattern of DC shift/SPC as recorded at a different time']. These criteria have recently been shown to improve ECoG scoring of SDs in high-artifact recordings [34].

This process resulted in the selection of Prototype device channel data that could be compared with time-matched ECoG DC-shifts.

Scalp and ECoG DC-shift curve fitting, comparison, visualization, and spatial extent

The scalp and ECoG data was processed via a curve fitting procedure designed to provide equivalent flat baselines and create curve-fitting parameters to define and quantitatively compare their time-courses. Given that the two signals from the ECoG strip and CerebroPatch™ Proof-of-Concept Prototype device were collected with different sensors and with different background interferences, this processing enables them to be quantitatively compared on an "equal" basis, as if there were recorded under exactly the same conditions. This processing involved subtracting a fitted baseline, fitting each data set to a Gaussian, and scaling the Prototype device data with the ratio of the maximum voltage extents. This procedure allowed the quantitative comparison, not only of the fitted parameters as shown in Table 1, but also the comparison of time-courses via the square of the correlation coefficient, the Coefficient-of-Determination (CoD). To implement this quantitative comparison of the Prototype device readable DC-shifts and ECoG DC-shifts coded as SDs, an epoch width that captured the entire DC-shift and included sufficient regions of stable baseline was chosen. The average DC-voltages in the eight second segments within each of these epochs of the 29 Prototype device and 6 ECoG channels were fitted using least squares to a six parameter model: three parameters for a Gaussian function model characterized by amplitude, width (or 'sigma'), and the maximum signal time and three parameters for a quadratic baseline consisting of a DC offset, a DC linear drift, and a second-order DC drift. The ECoG and Prototype device channels with the maximum amplitude (largest deviations from zero) were used to compare their respective peak DC-shifts. The ratio of the maximum amplitudes was used to scale the 8 second binned Prototype device signals to that of the ECoG signal to compute the CoD for the comparison of their structural similarity. A CoD value of >0.80 was deemed as suggesting acceptable similarity. The Gaussian parameters of signal amplitude, time of the peak signal, the full-width-half-maximum (FWHM), as 2.355 x sigma, and frequency as 1/FWHM were used to compare the Prototype device and ECoG DC-shifts.

The spatial extent of the scalp voltage field detected by the Prototype device from the brain-surface SDs was estimated as the area of the contiguous region above the 50% isocontour of the DC-voltage amplitude at the peak voltage time and the diameter of a circle with the equivalent area.

Statistics

Statistical tests were performed using SAS/STAT version 15.1 (SAS institute Inc, Cary, NC). Parametric or nonparametric statistical tests were used appropriately depending on the Shapiro-Wilk test for normality. Outliers were not excluded as SDs vary widely depending on their surrounding metabolic and circulatory milieu. Different measures of central tendency are reported depending on the Shapiro-Wilk test: the mean ± standard deviation (StD) or the median [interquartile range, IQR]. A 2-sided p value of less than 0.05 was accepted as statistically significant.

Results

Skin irritation scores, study interruptions and usability

The only instance of the skin irritation scores being other than zero was a score of 2 (erythema) recorded after 6 days for one subject. The CerebroPatch™ Proof-of-Concept Prototype was removed and data collection halted. In one subject, skin depressions ("bumps") at the electrode sites were noted during the re-gelling procedure but subsided over an hour. For another subject, the Prototype device was removed and data collection halted after 7 days due to family complaints. There were multiple adhesion issues reported in 7 out of 10 patients with many comments in the data sheets describing difficulties due to the device not sticking to the scalp after its removal and re-application for daily skin

irritation assessment and for imaging procedures.

Joint ECoG and CerebroPatch™ Proof-of-Concept Prototype analysis

None of the data from Cohorts 1 and 3 was available due to excessive artifacts. Out of the five subjects in Cohort 2, two had no identifiable ECoG SDs and two had excessive artifacts in the Prototype device signals. Data analysis focused on one 66-to-70-year-old female sub-arachnoid hemorrhage patient with 140 SDs and ISDs identified from the LabChart analysis of the ECoG data over a period of 11 days at which time the patient was discharged to in-patient rehabilitation. In this 11 day period, there were 0.85 days of readable Prototype device data with 1.84 days of no recording and 8.31 days of unreadable Prototype device signals. All 140 of these LabChart identified SDs and ISDs were visualized using the Python script depiction of the ECoG voltage time series. From this analysis, these ECoG-coded SDs and ISDs exhibited multi-ECoG electrode DC-shifts.

Of these 140 ECoG-coded SDs and ISDs, 38 could be visualized in both the Prototype device channel plots and the movies, but just 26 of these were deemed readable in the Prototype device recordings. Notably some of these 26 epochs exhibited minimal artifacts during their DC-shifts but were still deemed readable. Gaussian plus baseline curve fitting with 4-min epoch widths was performed for 24 of these 26 DC-shifts, with 2 epochs fitted with 12 min widths. The parameter fitting errors of all of the 26 Prototype device and 26 ECoG peak signal epochs were under 11%, although in one of these 26 epochs some of the 8-sec bin values were removed due to obvious artifacts.

DC-shift comparison and characterization

The CoD of corresponding 8-second segments from all 26 of the ECoG and CerebroPatch™ Proof-of-Concept Prototype DC-shifts was calculated to enable their comparison. The histogram of these CoDs is shown in Figure 3A. Two of these 26 epochs had CoDs less than 0.80 thus excluding them from further analysis based on a lack of similarity. The CoD of one of these was 0.797, because noisy portions of the time courses were excluded from the fitting procedure. This process left 24 DC-shifts that were deemed structural similar. The median [IQR] CoD of the 24 scaled Prototype device and ECoG DC-shifts that met the 0.80 limit of similarity was 0.98 [0.02], n = 24. The Gaussian fit parameters of the DC-shifts in these 24 epochs are presented in Table 1.

The CerebroPatch™ Proof-of-Concept Prototype-visible DC-shifts were characterized by peak DC-voltages of -457 ± 69 μV, n = 24, in comparison to the ECoG voltage of -3771 ± 171 μV, n = 24, with a voltage ratio of 0.121 ± 0.016, n = 24. The duration expressed as the FWHM of the fitted curves of the ECoG and Prototype device DC-shifts was 63.2 ± 3.65 sec, n = 24, and 70.9 ± 5.92 sec, n = 24, ($p<0.001$, paired t-test), respectively, with the Prototype device duration being longer presumably because of the spread of the electric field as it travelled through the layers from the brain to the scalp. The time of the Prototype device peak was delayed compared to the ECoG peak by a median of 2.89 [2.32] sec, n = 23 sec (with one preceding removed). This delay was much less than the sampling time of 8 seconds and corresponds to 4.3% of the average duration.

SD cluster and structural comparison

The raw data from the ECoG strip and CerebroPatch™ Proof-of-Concept Prototype from a cluster of 5 DC-shifts are presented in Figure 2A and 2B, respectively, after being down-sampled into 8-sec data blocks. This cluster of five DC-shifts was part of a cluster of 25 DC-shifts that occurred over a period of 8.25 hr with a mean interval of 22.4 ± 0.4 min, n = 24. Their DC-shifts appeared in a similar configuration of Prototype device electrodes. Figure 3B shows the structural similarity of the processed data derived from the 8-second binned raw ECoG and Prototype device data of the 3rd of the 5 DC-shifts presented in Figures 2A and 2B. This structural similarity is demonstrated by a CoD of 0.98.

Spatial extent

Although the time-courses of the ECoG and CerebroPatch™ Proof-of-Concept Prototype DC-shifts match at the electrode level, the brain-surface DC-potential of the SD spatially spreads as it travels through the various tissues to the scalp [7]. The wide spatial spread of the Prototype device DC-shifts on the scalp was characterized by an area of 18.7 ± 2.76 cm^2, n = 24, that encompassed the region

within the 50% isocontour and a diameter of a circle with the equivalent area of 4.87 ± 0.365 cm, n = 24. The 4-5 cm extent of the scalp DC-shift at the peak at 4:51 min:sec is shown in Prototype device image in Figure 2C.

EEG suppression

Although several attempts were made to replicate the EEG suppression observed in the ECoG recordings in the CerebroPatch™ Proof-of-Concept Prototype channel plots and movies, we were not able to achieve this analysis. Replicating the bipolar analysis used to improve the observation of EEG suppression in ECoG recordings from the multiple signals in a closely-spaced 2D electrode array such as the Prototype device is not straightforward.

CerebroPatch™ Proof-of-Concept Prototype video

For this same epoch of 5 DC-shifts shown in Figures 2A and 2B, Supplemental Video S1 shows the ECoG and Prototype device channel plots, their similar time courses, and a heat-map movie of the 3rd of the 5 DC-shifts with its rapid depression and recovery with a FWHM of 63.6 sec that reaches a minimum of -410 μV. The extent of this DC-shift includes Prototype device electrodes A4, A5, B4, B5, B6, C5, C6, C7, D4, and D5 and covers an area of 19.91 cm^2 with its associated diameter of 5.04 cm at its maximum deviation time of 4:51 min:sec. A slight DC-shift that rises and falls at some of the same Prototype device electrodes A5, B5, and B6 with amplitude of approximately -80 μV is visible that is time-locked to the DC-shift from ECoG electrode #4 at 4:56 min:sec.

Discussion

Noninvasive SD detection is possible using scalp DC-potentials

The main findings of this study are: 1) artifact issues limited the analysis to 10% (0.85/8.31 days) of the recording time in one patient and did not allow data analysis in the other 2 Cohort 2 patients with ECoG-identifiable SDs; 2) Usability was severely limited by the necessity of the re-gelling procedure and the inadequacy of the scalp adhesion system; 3) the DC-shifts of brain-surface SDs can be detected from the scalp; 4) the scaled scalp DC-shifts from the CerebroPatch™ Proof-of-Concept Prototype and those from the gold-standard ECoG SDs are almost identical as indicated by their matching curve parameters and CoDs greater that 0.80; 5) the extent of the scalp DC-potential is consistent with its spread during its passage from the brain surface to the scalp as estimated using numerical simulation; and 6) the scalp/brain voltage ratio is higher than previous estimates. These findings are tempered as they occurred in one subject with one specific and unusual SD pattern consisting of large nearly isoelectric DC-shifts that spread to adjacent channels as both DC-shifts and EEG suppression.

The structural similarity of the invasively recorded DC-shifts identified as SDs from the gold-standard ECoG method [20, 21] and the noninvasively recorded DC-shifts from the CerebroPatch™ Proof-of-Concept Prototype was assessed by a processing procedure that allowed for their quantitative comparison. The similarity of 24 of 26 DC-shifts with a CoD greater than 0.80 is documented by a median [IQR] CoD of 0.98 [0.02] as presented in Table 1 with an example shown in Figure 3B. This numerical comparison of the invasively and noninvasively detected DC-shifts and the visualization and spatial characterization as enabled by our closely-spaced 1-cm electrode array distinguishes our results from previous scalp DC-shift recordings [6, 27]. Their more widely spaced scalp electrode placements did not permit the reconstruction and visualization of the scalp electric field or allow the optimal alignment of the scalp and brain surface electrodes for the quantitative comparison of their DC-shifts.

This quantitative evidence of similarity gives support to the suggestion that this proof-of-concept validation data of noninvasive SD detection can lead to the implementation of clinically useful SD detection. However, the artifact and usability issues of the proof-of-concept Prototype device need to be overcome for noninvasive DC-EEG-based SD detection to be widely adopted. If these issues can be corrected in a future design then artifact-free and user-friendly noninvasive SD detection using DC-EEG could be used for evaluating brain-saving SD-based therapies to improve outcomes in sABI patients by mitigating the effects of secondary brain injury.

Scalp/brain DC-shift voltage ratio

The results of our numerical simulations of concussive-SD [7] and the globular SDs of sABI's [67] were helpful in associating the scalp DC-potentials with ECoG coded SDs. However our scalp/brain voltage ratio of 0.121 is larger than our previous values of 0.0735 from concussive-SD numerical simulation [7] and 0.0316 from Drenckhahn et al.'s [6] SAH patient data presented by Hund et al. [7]. The differences between these ratios can be attributed to several factors, including SD morphology differences (as presented previously [7]), skull thickness variations, and brain/scalp electrode mis-alignment.

The scalp/brain voltage ratio of an SD is highly dependent on skull thickness. Our simulation results showed that 44% of the voltage drop between the brain surface and the scalp occurs due the resistivity of the skull [7], so variations in skull thickness have a major effect of the voltage ratio. From the simulation data of Hund et al. [7], the ratio would increase from 0.0735 to 0.109 (by 49%) if the estimated skull thickness of 5.7 mm was reduced by 0.5 mm (by 9%), emphasizing how important skull thickness and its resistivity is to the scalp/brain ratio. Skull thickness is highly variable both within [68] and between individuals with coefficients of variation from 20 to 32% [69, 70].

The Drenckhahn et al. [6] ratio of 0.316 reported in Hund et al. [7] was from a comparison of various locations of brain surface and scalp electrode positions that were not aligned to provide positions that sampled equivalent regions of the SD's voltage field at the brain surface and scalp. In addition, the skull thickness differences from the various scalp electrode positions could potentially result in more resistive lowering of the scalp voltage than for our data, and therefore a lower voltage ratio, whereas our ratio of 0.121 was calculated from the maximum voltages from each electrode location, be it brain surface or scalp.

SD identification criteria by different methods

We suggest that the gold-standard ECoG method for SD identification [20, 21] is method-based and our 1-cm spaced DC-EEG electrode scalp method might have different SD identification criteria. This conjecture is supported by more than several examples of SD identification criteria other than those used for the invasive ECoG method that is considered to be the gold-standard [20, 21]. Invasive SD identification efforts began with the initial observation by Mayevsky et al. [71] of multiple SDs at one location identified with invasive continuous multi-parametric on-line monitoring of cerebral blood flow and volume, intramitochondrial NADH redox state, extracellular K^+ concentration, intracranial pressure, cortical DC field potential, and ECoG from localized bipolar electrodes [71]. In this instance, changes in multiple primary and secondary SD parameters give confidence of proper SD identification without the necessity or inclusion of propagation. Hadjikhani et al. [8] used fMRI signal changes that demonstrated at least eight, mostly secondary, characteristics of SD that were time-locked to migraine aura to strongly suggest that an electrophysiological event such as SD generates the aura. Strong et al. [17] used only EEG suppression and its propagation to identify SDs in their introduction of the now widely accepted invasive 6-electrode ECoG strip method. Other modalities completely independent from any primary SD characteristics have been used to identify SDs in humans and experimental models. These include changes in laser speckle flowmetry and intrinsic optical change along with their propagation [15], NADH fluorescence changes [72], and MRI characteristics such as decreases in the apparent diffusion coefficient [73, 74]. Another method of SD identification was presented by Bastany et al. [33] who identified SDs using scalp EEG with similar curve comparison methods to our use of the CoD, but only between near-DC recorded scalp potentials, not between ECoG and scalp DC-shifts as performed here.

Support for noninvasive SD identification criteria, beyond those set forth by COSBID using invasive ECoG [20, 21], are provided by Hartings et al. [31] who stated that,

> "[N]o criteria for definitive diagnosis of SDs by scalp EEG has yet been proposed. [Although the] criteria for ECoG recordings from the brain surface using subdural electrodes … have been firmly established [20] [it] is unlikely that these criteria could also be applied in a straightforward manner for SD identification in scalp EEG."

This quote augurs several efforts to explore noninvasive SD detection using clinical frequency EEG

with ~2.5 cm electrode spacing that have focused on providing an algorithm to assess the width and duration of SD's secondary EEG suppression as SD identification criteria [28, 29, 75]. These approaches based on EEG suppression are distinct compared to this current proof-of-concept human study using DC-EEG to explore noninvasive SD detection of the primary DC-shift of an SD. We justify our focus on DC-EEG for noninvasive SD detection because of its importance in identifying the primary attribute of SD. The importance of DC-EEG for SD identification is in contrast to its lack of acceptance for diagnostic clinical EEG.

These previously mentioned studies used multiple criteria for identifying SDs depending on the detection method. The comparison and validation system presented here using quantitative comparison of fitted DC-shift curve parameters from channels with maximum voltages combined with the representation of the spatial distribution of the scalp DC-potential suggests another method of SD identification. This method would focus on a limited, artifact-free 4-min period that encompasses a suspected DC-EEG signal of a SD which can be analyzed quantitatively to identify a SD via the magnitude, duration, and spatial extent of its characteristic DC-shift.

Device-design based limitations: Impact of artifacts and usability on SD identification

The CerebroPatch™ Proof-of-Concept Prototype's ability to gather artifact-free data was severely limited. Only one patient had acceptable artifact-free periods that were appropriate for data analysis based on visual readability. Many of the ECoG-coded SDs in this data set were obscured by artifacts due to inherent limitations in the design of the Prototype device. This artifact burden suggests that additional of proof-of-concept validation studies are necessary for a DC-EEG system that improves usability and reduces artifacts to make noninvasive SD detection widely available. A radically different device design could well eliminate or minimize the Prototype device-based limitations of artifact burden and lack of usability. It is unclear, and subject to additional observations, as to whether a new design would enable observation of DC-shift propagation and EEG suppression at the scalp and confirm this DC-shift-based proof-of-concept observation that the DC signal from closely-spaced scalp-placed electrodes provide of noninvasive SD detection.

Observational limitations: lack of propagation and EEG suppression

The limitations of this proof-of-concept noninvasive study include not observing DC-shift propagation or EEG suppression in the DC-shift scalp recordings. The Prototype device movies created from Gaussian radial-basis function interpolation of the 2D array of DC-potentials [65, 66] were capable of visualizing potential propagation, but did not provide evidence of propagation. The Prototype device image movies do show DC-shifts that are synchronous with the ECoG DC-shifts that were coded as SDs by an experienced reader. These DC-shifts appear in one contiguous region and then dissipate without apparent propagation in scalp recordings, but clearly demonstrated propagation on the ECoG recordings that is more noticeable in the high frequency recording of EEG suppression. This lack of propagation in the scalp recordings could be because of:

1. The propagation could have occurred out of the region covered by the Prototype device's electrode array;
2. The propagation of a subsequent SD in this cluster could be suppressed by the refractory period caused of the previous SD [76]; or
3. Given that the evidence for propagation was mostly in the EEG suppression signal, the inability to observe EEG suppression in the scalp array could limit our ability to observe it.

There is a possibility that the lack of scalp DC-shift propagation did actually reflect cortical non-spreading depolarizations as the preponderance of evidence for propagation was from EEG suppression. This conjecture is supported by observations of cortical non-spreading depressions [17] and depolarizations [33, 40]. In the first human observation of spreading depression with the ECoG strip methodology [17], 20% of the 48 spreading depressions were estimated to be "stationary" based on subtracting the estimated number that would be deemed as to have travelled perpendicular to the ECoG strip. Dohmen et al. [40] specifically mentions not reporting 65 slow potential changes associated with SDs that "did not show clear spread of depolarizations" to abide by the criteria that "specify spread

of depolarization as a prerequisite" for scoring an SD. Bastany et al. [33] also observed "stationary" cortical depolarizations. Kager et al. [77] modeled the core process of spreading depolarization in a single neuron, suggesting that propagation is not an essential feature of spreading depolarization [3]. One possibility that supports this modeling conjecture is that the mechanism for SD propagation, as separate from the mechanism for initiation [38], could have been selectively impaired. We surmise non-propagating SDs are underreported by investigators because they are presumed to be traveling perpendicular to the ECoG strip, are classed inappropriately as artifacts, or are dismissed as missing one of the presumed essential identifiers of SDs.

If these non-spreading depolarizations exist, they may be part of the heterogeneity of electric field spatial and temporal characteristics as suggested by the simulations of Herreras et al. [78]. This heterogeneity includes the expanding rings of concussive SDs, the radiating centripetally expanding ring of the initial SD of stroke, and the globular SDs associated with sABI. Traveling globular SDs of sABI exhibit heterogeneity of duration both in humans [79] and experimentally [80, 81] with their duration lengthening as tissue deteriorates.

Effect of ECoG strip on SD voltage field propagation

Our numerical simulation of an SD passing under an ECoG strip [67] showed that the surface signal is increased by 19% when passing under the platinum electrodes in the ECoG strip or diminished by 8% when it passes under their silastic encasement. These simulation results suggest that SDs can be detected even if they pass under the ECoG strip and that the increase in signal when the SD passes under the platinum electrode portion of the ECoG strip was not large enough to suggest that our SD detection was dependent on this increase. Therefore, we are confident SD detection by the CerebroPatch™ Proof-of-Concept Prototype was not dependent on, or inhibited by, the presence of conductive properties of the ECoG strip, nor obscured by its resistive elements.

Conclusions

Despite the limitations of this proof-of-concept study, we showed that the time-matched CerebroPatch™ Proof-of-Concept Prototype scalp DC-shifts originate from SDs validated using the COSBID identification criteria [20, 21]. In addition, the spatial characteristics of the CerebroPatch™-detected DC-shifts are consistent with the spread of the brain-surface DC-potential from a SD. These results suggest that the Prototype device DC-shifts are from SDs and that noninvasive SD detection is possible using scalp DC-potential signals. Although the Prototype device SD identification procedures depended on SD identification using the ECoG strip gold-standard, they did enable the proof-of-concept validation that the Prototype device was capable of identifying SDs.

We suggest that effective noninvasive SD detection in the neuro-ICU environment needs an easily applied electrode array design with provisions for robust scalp adhesion that provides a stable skin-electrode interface to minimize artifacts, can be used for extended periods without the need for reapplication, and that is not irritating to the skin.

Acknowledgements

We are grateful for the technical assistance provided by Nicholas Urioste, Amal Alchbli, and Mohammad Abbas and to Mihika Gangolli for the suggestion to use the Coefficient-of-Determination to compare DC-shifts. We thank Thomas Ferguson, Rebekah Kummer, and Joel Greenberg for reading and commenting on the manuscript. We acknowledge support from the Ansys StartUp Program and the Duquesne University Small Business Development Center.

Funding

This project was conducted for CerebroScope, a medical device company developing a scalp DC-EEG system for detecting SDs in sABI, concussion, and migraine. This work was partially supported by grants from the: US Public Health Service National Institutes of Health: NS30839, NS30839-14S1 and NS66292 to the SCJ while at the Allegheny-Singer Research Institute; and 5R43NS092181 and 3R43NS092181-02S1 to SCJ for CerebroScope.

Competing Interests

Stephen C. Jones and Samuel J. Hund are founding partners and shareholders of CerebroScope. Benjamin R. Brown is a consultant to and shareholder of CerebroScope, Eric L. Singer is a shareholder, and Andrew P. Carson is a previous shareholder of CerebroScope.

Compliance with Ethical Standards

All ethical standards have been met. See section “Human study issues”.

Intellectual Property Disclosures

Parts of this work are disclosed in: U.S. Patent No. 10,028,694 published and publically available on May 26, 2016 and issued July 24, 2018; U.S. Patent No. US11234628B2 issued February 1, 2022; and European Patent No. 3223693 issued February 28, 2024.

Supplementary material

Supplementary material is available at the journal’s website.

References

1. Grafstein B. Locus of propagation of spreading cortical depression. J Neurophysiol. 1956;19:308-316, PMID:PM:13332438. Ref ID: 222300

2. Leao AAP. Spreading depression of activity in the cerebral cortex. J Neurophysiol. 1944;7:359-390, https://doi.org/10.1152/jn.1944.7.6.359, PMID:Not in Pubmed. Ref ID: 10479

3. Dreier JP. The role of spreading depression, spreading depolarization and spreading ischemia in neurological disease. Nat Med. 2011;17:439-447, PMID:PM:21475241. Ref ID: 222877

4. Lauritzen M, Dreier JP, Fabricius M, Hartings JA, Graf R, Strong AJ. Clinical relevance of cortical spreading depression in neurological disorders: migraine, malignant stroke, subarachnoid and intracranial hemorrhage, and traumatic brain injury. J Cereb Blood Flow Metab. 2011;31:17-35, PMID:PM:21045864. Ref ID: 222261

5. Leao AA. The slow voltage variation of cortical spreading depression of activity. Electroencephalogr Clin Neurophysiol. 1951;3:315-321, PMID:PM:14879782. Ref ID: 222699

6. Drenckhahn C, Winkler MK, Major S, et al. Correlates of spreading depolarization in human scalp electroencephalography. Brain. 2012;135:853-868, PMID:PM:22366798, PMCID:PMC3286336. Ref ID: 223472

7. Hund SJ, Brown BR, Lemale CL, et al. Numerical Simulation of Concussive-generated Cortical Spreading Depolarization to Optimize DC-EEG Electrode Spacing for Non-invasive Visual Detection. Neurocrit Care. 2022;37:S67-S82, PMID:PM:35233716, PMCID:PMC9262830. Ref ID: 224957

8. Hadjikhani N, Sanchez Del Rio M, Wu O, et al. Mechanisms of migraine aura revealed by functional MRI in human visual cortex. Proc Natl Acad Sci USA. 2001;98:4687-4692, PMID:PM:11287655. Ref ID: 21643

9. Major S, Huo S, Lemale CL, et al. Direct electrophysiological evidence that spreading depolarization-induced spreading depression is the pathophysiological correlate of the migraine aura and a review of the spreading depolarization continuum of acute neuronal mass injury. Geroscience. 2020;42:57-80, PMID:PM:31820363, PMCID:PMC7031471. Ref ID: 228432

10. Bouley J, Chung DY, Ayata CY, Brown RH, Jr., Henninger N. Cortical spreading depression denotes concussion injury. J Neurotrauma. 2019;36:1008-1017, PMID:PM:29999455, PMCID:PMC6444888. Ref ID: 227151

11. Pacheco JM, Hines-Lanham A, Stratton C, et al. Spreading Depolarizations Occur in Mild Traumatic Brain Injuries and Are Associated with Postinjury Behavior. eNeuro. 2019;6:1-17, PMID:PM:31748237. Ref ID: 227920

12. Colpitts K, Desai MJ, Kogan M, Shuttleworth CW, Carlson AP. Brain Tsunamis in Human High-Grade Glioma: Preliminary Observations. Brain Sci. 2022;12, PMID:PM:35741596, PMCID:PMC9221439. Ref ID: 229453

13. Curry RN, Aiba I, Meyer J, et al. Glioma epileptiform activity and progression are driven by IGSF3-mediated potassium dysregulation. Neuron. 2023;111:682-695, PMID:PM:36787748, PMCID:PMC9991983. Ref ID: 230328

14. Street JS, Lignani G. A Salt in the Buffer Zone: Potassium Dysregulation Drives Glioma Growth? Epilepsy Curr. 2023;23:309-311, PMID:PM:37901777, PMCID:PMC10601028. Ref ID: 230330

15. Woitzik J, Hecht N, Pinczolits A, et al. Propagation of cortical spreading depolarization in the human cortex after malignant stroke. Neurology. 2013;80:1095-1102, PMID:PM:23446683. Ref ID: 224397

16. Fabricius M, Fuhr S, Bhatia R, et al. Cortical spreading depression and peri-infarct depolarization in acutely injured human cerebral cortex. Brain. 2006;129:778-790, PMID:PM:16364954. Ref ID: 24597

17. Strong AJ, Fabricius M, Boutelle MG, et al. Spreading and synchronous depressions of cortical activity in acutely injured human brain. Stroke. 2002;33:2738-2743, PMID:PM:12468763. Ref ID: 20804

18. Dreier JP, Major S, Manning A, et al. Cortical spreading ischaemia is a novel process involved in ischaemic damage in patients with aneurysmal subarachnoid haemorrhage. Brain. 2009;132:1866-1881, PMID:PM:19420089, PMCID:PMC2702835. Ref ID: 25880

19. Voorhies JM, Cohen-Gadol A. Techniques for placement of grid and strip electrodes for intracranial epilepsy surgery monitoring: Pearls and pitfalls. Surg Neurol Int. 2013;4:98, PMID:PM:23956941, PMCID:PMC3740610. Ref ID: 228448

20. Dreier JP, Fabricius M, Ayata C, et al. Recording, analysis, and interpretation of spreading depolarizations in neurointensive care: Review and recommendations of the COSBID research group. J Cereb Blood Flow Metab. 2017;37:1595-1625, PMID:PM:27317657. Ref ID: 226756

21. Hartings JA, Li C, Hinzman JM, et al. Direct current electrocorticography for clinical neuromonitoring of spreading depolarizations. J Cereb Blood Flow Metab. 2017;37:1857-1870, PMID:PM:27286981. Ref ID: 226768

22. Meinert F, Lemâle CL, Major S, et al. Less-invasive subdural electrocorticography for investigation of spreading depolarizations in patients with subarachnoid hemorrhage. Front Neurol. 2022;13:Online ahead of print, PMID:PM:36686541, PMCID:PMC9849676. Ref ID: 229754

23. Meinert F, Dömer P, Helgers SOA, et al. Subdural Placement of Electrocorticographic Electrode Array Through a Burr Hole Exposure: 2-Dimensional Operative Video. Oper Neurosurg (Hagerstown). 2022;23:e169, PMID:PM:35972097. Ref ID: 229457

24. Foreman B, Ngwenya LB, Stoddard E, Hinzman JM, Andaluz N, Hartings JA. Safety and Reliability of Bedside, Single Burr Hole Technique for Intracranial Multimodality Monitoring in Severe Traumatic Brain Injury. Neurocrit Care. 2018;29:469-480, PMID:PM:29949001. Ref ID: 227157

25. Jeffcote T, Hinzman JM, Jewell SL, et al. Detection of spreading depolarization with intraparenchymal electrodes in the injured human brain. Neurocrit Care. 2014;20:21-31, PMID:PM:24343564. Ref ID: 225652

26. Hartings JA, Andaluz N, Bullock MR, et al. Prognostic Value of Spreading Depolarizations in Patients With Severe Traumatic Brain Injury. JAMA Neurol. 2020;77:489-499, PMID:PM:31886870, PMCID:PMC6990808. Ref ID: 227886

27. Hartings JA, Wilson JA, Hinzman JM, et al. Spreading depression in continuous electroencephalography of brain trauma. Ann Neurol. 2014;76:681-694, PMID:PM:25154587. Ref ID: 225976

28. Chamanzar A, Elmer J, Shutter L, Hartings J, Grover P. Noninvasive and reliable automated detection of spreading depolarization in severe traumatic brain injury using scalp EEG. Commun Med (Lond). 2023;3:113, PMID:PM:37598253, PMCID:PMC10439895. Ref ID: 229998

29. Wu Y, Jewell S, Xing X, et al. Real-Time Non-Invasive Imaging and Detection of Spreading Depolarizations through EEG: An Ultra-Light Explainable Deep Learning Approach. IEEE J Biomed Health Inform. 2024;28:5780-5791, PMID:PM:38412076. Ref ID: 230247

30. Hofmeijer J, van Kaam CR, van de Werff B, Vermeer SE, Tjepkema-Cloostermans MC, van Putten MJAM. Detecting Cortical Spreading Depolarization with Full Band Scalp Electroencephalography: An Illusion? Front Neurol. 2018;9, PMID:PM:29422883. Ref ID: 227039

31. Hartings JA, Ngwenya LB, Watanabe T, Foreman B. Commentary: Detecting Cortical Spreading Depolarization with Full Band Scalp Electroencephalography: An Illusion? Front Syst Neurosci. 2018;12, PMID:PM:29869634, PMCID:PMCID: PMC5964196. Ref ID: 227159

32. Robinson D, Hartings J, Foreman B. First Report of Spreading Depolarization Correlates on Scalp EEG Confirmed with a Depth Electrode. Neurocrit Care. 2021;35:100-104, PMID:PM:34617254. Ref ID: 228984

33. Bastany ZJR, Askari S, Dumont GA, Kellinghaus C, Kazemi A, Gorji A. Association of cortical spreading depression and seizures in patients with medically intractable epilepsy. Clin Neurophysiol. 2020;131:2861-2874, PMID:PM:33152524. Ref ID: 229193

34. Fritch CD, Qeadan F, Shuttleworth CW, Carlson AP. Spreading depolarization occurs in repeating, recognizable, patient-specific patterns after human brain injury. Brain Inj. 2021;35:299-303, PMID:PM:33529080. Ref ID: 228726

35. Chamanzar A, George S, Venkatesh P, et al. An algorithm for automated, noninvasive detection of cortical spreading depolarizations based on EEG simulation. IEEE Trans Biomed Eng. 2019;66:1115-1126, PMID:PM:30176578. Ref ID: 227272

36. Belur PK, Chang JJ, He S, Emanuel BA, Mack WJ. Emerging experimental therapies for intracerebral hemorrhage: targeting mechanisms of secondary brain injury. Neurosurg Focus. 2013;34:E9, PMID:PM:23634928. Ref ID: 229843

37. Bramlett HM, Dietrich WD. Long-Term Consequences of Traumatic Brain Injury: Current Status of Potential Mechanisms of Injury and Neurological Outcomes. J Neurotrauma. 2015;32:1834-1848, PMID:PM:25158206, PMCID:PMC4677116. Ref ID: 229760

38. Pietrobon D, Moskowitz MA. Chaos and commotion in the wake of cortical spreading depression and spreading depolarizations. Nat Rev Neurosci. 2014;15:379-393, PMID:PM:24857965. Ref ID: 225848

39. Hartings JA, Rolli ML, Lu XC, Tortella FC. Delayed secondary phase of peri-infarct depolarizations after focal cerebral ischemia: relation to infarct growth and neuroprotection. J Neurosci. 2003;23:11602-11610, PMID:PM:14684862. Ref ID: 24984

40. Dohmen C, Sakowitz OW, Fabricius M, et al. Spreading depolarizations occur in human ischemic stroke with high incidence. Ann Neurol. 2008;63:720-728, PMID:PM:18496842. Ref ID: 25873

41. Hartings JA, Bullock MR, Okonkwo DO, et al. Spreading depolarisations and outcome after traumatic brain injury: a prospective observational study. Lancet Neurol. 2011;10:1058-1064, PMID:PM:22056157. Ref ID: 223098

42. Lemale CL, Lückl J, Horst V, et al. Migraine Aura, Transient Ischemic Attacks, Stroke, and Dying of the Brain Share the Same Key Pathophysiological Process in Neurons Driven by Gibbs-Donnan Forces, Namely Spreading Depolarization. Front Cell Neurosci. 2022;16:837650, PMID:PM:35237133, PMCID:PMC8884062. Ref ID: 229411

43. Dreier JP, Winkler MKL, Major S, et al. Spreading depolarizations in ischaemia after subarachnoid haemorrhage, a diagnostic phase III study. Brain. 2022;145:1264-1284, PMID:PM:35411920. Ref ID: 229409

44. Kowoll CM, Schumm L, Gieffers A, et al. Duration of spreading depression is the electrophysiological correlate of infarct growth in malignant hemispheric stroke. J Cereb Blood Flow Metab. 2024;Online ahead of print, PMID:PM:38902207. Ref ID: 230354

45. Carlson AP, Abbas M, Alunday RL, Qeadan F, Shuttleworth CW. Spreading depolarization in acute brain injury inhibited by ketamine: a prospective, randomized, multiple crossover trial. J Neurosurg. 2018;130:1513-1519, PMID:PM:29799344. Ref ID: 227126

46. Sugimoto K, Nomura S, Shirao S, et al. Cilostazol decreases duration of spreading depolarization and spreading ischemia after aneurysmal subarachnoid hemorrhage. Ann Neurol. 2018;84:873-885, PMID:PM:30341966. Ref ID: 228053

47. Carlson AP, Alchbli A, Hänggi D, Macdonald RL, Shuttleworth CW. Effect of Locally Delivered Nimodipine Microparticles on Spreading Depolarization in Aneurysmal Subarachnoid Hemorrhage. Neurocrit Care. 2021;34:345-349, PMID:PM:32103439. Ref ID: 228900

48. Klass A, Sanchez-Porras R, Santos E. Systematic review of the pharmacological agents that have been tested against spreading depolarizations. J Cereb Blood Flow Metab. 2018;38:1149-1179, PMID:PM:29673289. Ref ID: 227296

49. Eikermann-Haerter K, Can A, Ayata C. Pharmacological targeting of spreading depression in migraine. Expert Rev Neurother. 2012;12:297-306, PMID:PM:22364328, PMCID:PMC3321647. Ref ID: 224681

50. Hauge AW, Asghar MS, Schytz HW, Christensen K, Olesen J. Effects of tonabersat on migraine with aura: a randomised, double-blind, placebo-controlled crossover study. Lancet Neurol. 2009;8:718-723, PMID:PM:19570717. Ref ID: 225221

51. Jansen-Olesen I, Tfelt-Hansen P, Olesen J. Animal migraine models for drug development: status and future perspectives. CNS Drugs. 2013;27:1049-1068, PMID:PM:24234657. Ref ID: 225211

52. Dahlof CG, Hauge AW, Olesen J. Efficacy and safety of tonabersat, a gap-junction modulator, in the acute treatment of migraine: a double-blind, parallel-group, randomized study. Cephalalgia. 2009;29 Suppl 2:7-16, PMID:PM:19723121. Ref ID: 225220

53. Goadsby PJ, Ferrari MD, Csanyi A, Olesen J, Mills JG. Randomized, double-blind, placebo-controlled, proof-of-concept study of the cortical spreading depression inhibiting agent tonabersat in migraine prophylaxis. Cephalalgia. 2009;29:742-750, PMID:PM:19222510. Ref ID: 225222

54. Lipton RB, Dodick DW, Silberstein SD, et al. Single-pulse transcranial magnetic stimulation for acute treatment of migraine with aura: a randomised, double-blind, parallel-group, sham-controlled trial. Lancet Neurol. 2010;9:373-380, PMID:PM:20206581. Ref ID: 225721

55. Costa C, Tozzi A, Rainero I, et al. Cortical spreading depression as a target for anti-migraine agents. J Headache Pain. 2013;14:62, PMID:PM:23879550, PMCID:PMC3728002. Ref ID: 224963

56. Chen SP, Ayata C. Novel Therapeutic Targets Against Spreading Depression. Headache. 2017;57:1340-1358, PMID:PM:28842982. Ref ID: 227155

57. Carney N, Totten AM, O'Reilly C, et al. Guidelines for the Management of Severe Traumatic Brain Injury, Fourth Edition. Neurosurgery. 2017;80:6-15, PMID:PM:27654000. Ref ID: 227046

58. Talving P, Karamanos E, Teixeira PG, et al. Intracranial pressure monitoring in severe head injury: compliance with Brain Trauma Foundation guidelines and effect on outcomes: a prospective study. J Neurosurg. 2013;119:1248-1254, PMID:PM:23971954. Ref ID: 228387

59. Okonkwo DO, Shutter LA, Moore C, et al. Brain Oxygen Optimization in Severe Traumatic Brain Injury Phase-II: A Phase II Randomized Trial. Crit Care Med. 2017;45:1907-1914, PMID:PM:29028696, PMCID:PMC5679063. Ref ID: 227045

60. Barsan WG, Shutter LA, Diaz-Arrastia RR, Yeatts S. Brain Oxygen Optimization in Severe TBI, Phase 3, Clinical Trial #: NCT03754114. 2020; https://clinicaltrials.gov/study/NCT03754114. Ref ID: 228234

61. Bernard F, Barsan W, Diaz-Arrastia R, Merck LH, Yeatts S, Shutter LA. Brain Oxygen Optimization in Severe Traumatic Brain Injury (BOOST-3): a multicentre, randomised, blinded-endpoint, comparative effectiveness study of brain tissue oxygen and intracranial pressure monitoring versus intracranial pressure alone. BMJ Open. 2022;12:e060188, PMID:PM:35273066, PMCID:PMC8915289. Ref ID: 229455

62. Howard G, Schwamm LH, Donnelly JP, et al. Participation in Get With The Guidelines-Stroke and Its Association With Quality of Care for Stroke. JAMA Neurol. 2018;75:1331-1337, PMID:PM:30083763, PMCID:PMC6248106. Ref ID: 230382

63. ISO/Technical Committee 194. ISO 10933-10, Biological evaluation of medical devices - Part 10: Tests for irritation and skin sensitization. 2010; International Organization for Standardization Geneva,, Switzerland, https://www.iso.org/standard/40884.html. Ref ID: 228742

64. Kemp B, Olivan J. European data format 'plus' (EDF+), an EDF alike standard format for the exchange of physiological data. Clin Neurophysiol. 2003;114:1755-1761, PMID:PM:12948806. Ref ID: 229407

65. Jager J, Klein A, Buhmann M, Skrandies W. Reconstruction of electroencephalographic data using radial basis functions. Clin Neurophysiol. 2016;127:1978-1983, PMID:PM:26971479. Ref ID: 228415

66. Yao D. High-resolution EEG mapping: a radial-basis function based approach to the scalp Laplacian estimate. Clin Neurophysiol. 2002;113:956-967, PMID:PM:12048057. Ref ID: 228417

67. Hund SJ, Brown BR, Jones SC. Noninvasive detection of globular cortical spreading depolarization: Prediction by numerical simulation. 2024. In preparation. Ref ID: 230298

68. Mahinda HAM, Murty OP. Variability in thickness of human skull bones and sternum – An autopsy experience. J Forensic Med Toxicol. 2009;26:26-31, PMID:Not in Pubmed. Ref ID: 225577

69. Strangman GE, Zhang Q, Li Z. Scalp and skull influence on near infrared photon propagation in the Colin27 brain template. Neuroimage. 2014;85 Pt 1:136-149, PMID:PM:23660029. Ref ID: 228958

70. Wendel K, VÃ¤isÃ¤nen J, Seemann G, Hyttinen J, Malmivuo J. The influence of age and skull conductivity on surface and subdermal bipolar EEG leads. Comput Intell Neurosci. 2010;2010:397272, PMID:PM:20130812, PMCID:PMC2814227. Ref ID: 230344

71. Mayevsky A, Doron A, Manor T, Meilin S, Zarchin N, Ouaknine GE. Cortical spreading depression recorded from the human brain using a multiparametric monitoring system. Brain Res. 1996;740:268-274, PMID:PM:8973824. Ref ID: 221394

72. Strong AJ, Harland SP, Meldrum BS, Whittington DJ. The use of in vivo fluorescence image sequences to indicate the occurrence and propagation of transient focal depolarizations in cerebral ischemia. J Cereb Blood Flow Metab. 1996;16:367-377, PMID:PM:8621741. Ref ID: 4524

73. Takano K, Latour LL, Formato JE, et al. The role of spreading depression in focal ischemia evaluated by diffusion mapping. Ann Neurol. 1996;39:308-318, PMID:PM:8602749. Ref ID: 8629

74. Yushmanov VE, Kharlamov A, Yutzy SR et al. 3D tracking of transient peri-infarct depolarizations in ischemic rat brain by fast ADC mapping. Program # 3063; International Society of Magnetic Resonance in Medicine: https://archive.ismrm.org/2012/3063.html. Ref ID: 223259

75. Wang HY, Liu X, Grover P, Chamanzar A. A Spatial-Temporal Graph Attention Network for Automated Detection and Width Estimation of Cortical Spreading Depression Using Scalp EEG. Annu Int Conf IEEE Eng Med Biol Soc. 2023;2023:1-4, PMID:PM:38082965. Ref ID: 230215

76. Herreras O, Somjen GG. Analysis of potential shifts associated with recurrent spreading depression and prolonged unstable spreading depression induced by microdialysis of elevated K+ in hippocampus of anesthetized rats. Brain Res. 1993;610:283-294, PMID:PM:8319090. Ref ID: 228431

77. Kager H, Wadman WJ, Somjen GG. Conditions for the triggering of spreading depression studied with computer simulations. J Neurophysiol. 2002;88:2700-2712, PMID:PM:12424305. Ref ID: 25870

78. Herreras O, Makarova J. Mechanisms of the negative potential associated with Leão's spreading depolarization: A history of brain electrogenesis. J Cereb Blood Flow Metab. 2020;40:1934-1952, PMID:PM:32580670, PMCID:PMC7786845. Ref ID: 229866

79. Milakara D, Grozea C, Dahlem M, et al. Simulation of spreading depolarization trajectories in cerebral cortex: Correlation of velocity and susceptibility in patients with aneurysmal subarachnoid hemorrhage. Neuroimage Clin. 2017;16:524-538, PMID:PM:28948141. Ref ID: 227163

80. Santos E, Sanchez-Porras R, Sakowitz OW, Dreier JP, Dahlem MA. Heterogeneous propagation of spreading depolarizations in the lissencephalic and gyrencephalic brain. J Cereb Blood Flow Metab. 2017;37:2639-2643, PMID:PM:28121215. Ref ID: 226937

81. Santos E, Scholl M, Sanchez-Porras R, et al. Radial, spiral and reverberating waves of spreading depolarization occur in the gyrencephalic brain. Neuroimage. 2014;99:244-255, PMID:PM:24852458. Ref ID: 226716

Tables

Table 1: SD characterization

Table 1. Comparison of CerebroPatch™ Proof-of-Concept Prototype with ECoG DC-shift curve fit parameters

		Signal origin				
Parameter	Units	CerebroPatch™ Proof-of-Concept Prototype device	ECoG	Ratio or Difference	Fraction of duration	n
Peak Voltage	(μV)	-457 ± 69	-3771 ± 171	0.121 ± 0.016	-	24
Duration (FWHM)*	(sec)	70.9 ± 5.92	63.2 ± 3.65	1.12 ± 0.076	-	24
Frequency	(Hz)	0.0063 ± 0.0005	0.0070 ± 0.0004	-	-	24
Peak Time Difference**	(sec)	-	-	2.89 [2.32]	4.3%	23
Area***	(cm^2)	18.7 ± 2.71				24
Diameter****	(cm)	4.86 ± 0.358	-	-	-	24
Coefficient-of-Determination (>0.80)*****	(-)	-	-	0.98 [0.02]	-	24

Values are mean ± StD or median [interquartile range, IQR]

Twelve of the 38 epochs were excluded from analysis due to lack of readability and 2 out of the remaining 26 for Coefficient-of-Determination criteria

* $p < 0.001$, paired t-test

** With only scalp delayed (excluding one preceding)

*** Area within the 50% of maximum voltage extent

**** Diameter of a circle with an area within the 50% isocontour

***** Based on 8-sec data averages

Figures with legends

Figure 1

Figure 1: CerebroPatch™ Proof-of-Concept Prototype: A, Top view showing the domes covering the 29 1-cm spaced Ag/AgCl electrodes with their attached conductors; B, Angled bottom view showing double-sided adhesive and gelled electrode pits; C, Target position of Prototype device on forehead.

Figure 2

Figure 2: The ECoG (Panel A, 3400 µV full-scale) and CerebroPatch™ Proof-of-Concept Prototype (Panel B, 680 µV full scale, negative is "up") channel plots (dead channels A2, D1, D6, E1-4 data removed) with the electrode labels along right edge for 5 time-matched ECoG SDs and DC-shifts from the forehead-placed Prototype device showing their temporal synchrony. The red vertical time marker is at the peak of the 3rd SD at 4:51. These SDs are part of the cluster of 25 SDs that have an inter-SD interval of 22 min. Panel C shows the Prototype device image at the 4:51 peak of the 3rd SD showing the extent of the SD at the scalp. The electrodes in Panel C are represented as small black circles labeled in five rows with 5 electrodes in rows A and E, 6 in rows B and D, and 7 in row C with a filled-circle depicting electrode A1. In the bottom panel the pseudo-color scale ranges from 250 to -410 µV (positive-negative reversed as negative is "up").

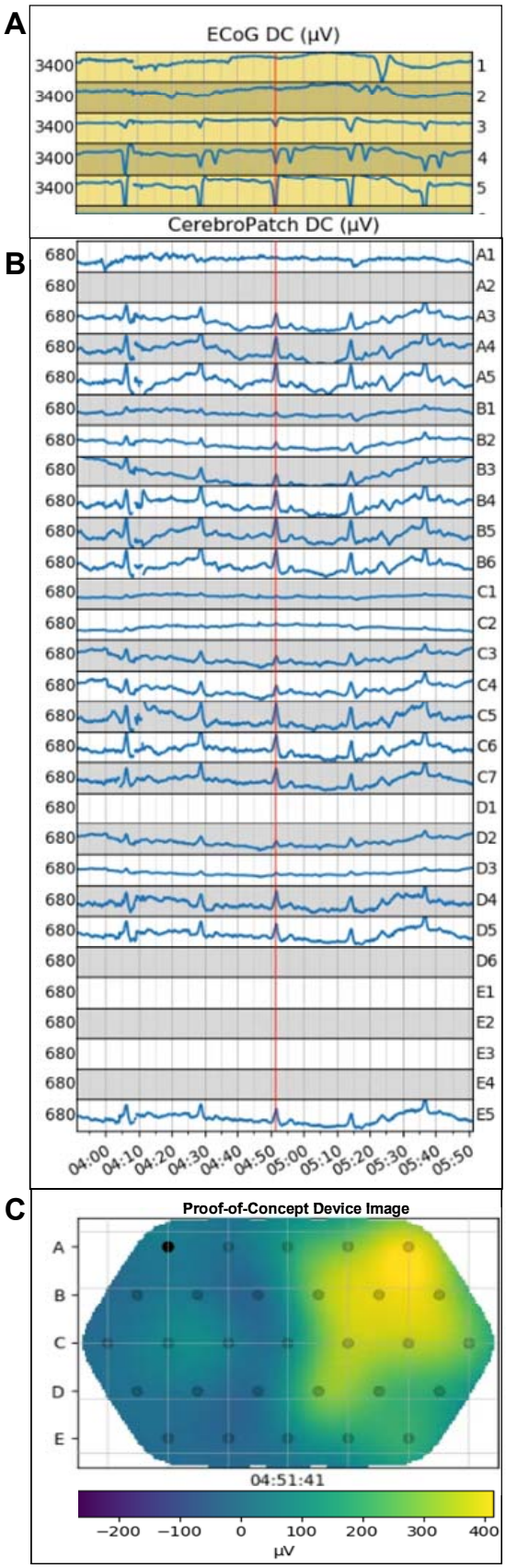

Figure 3

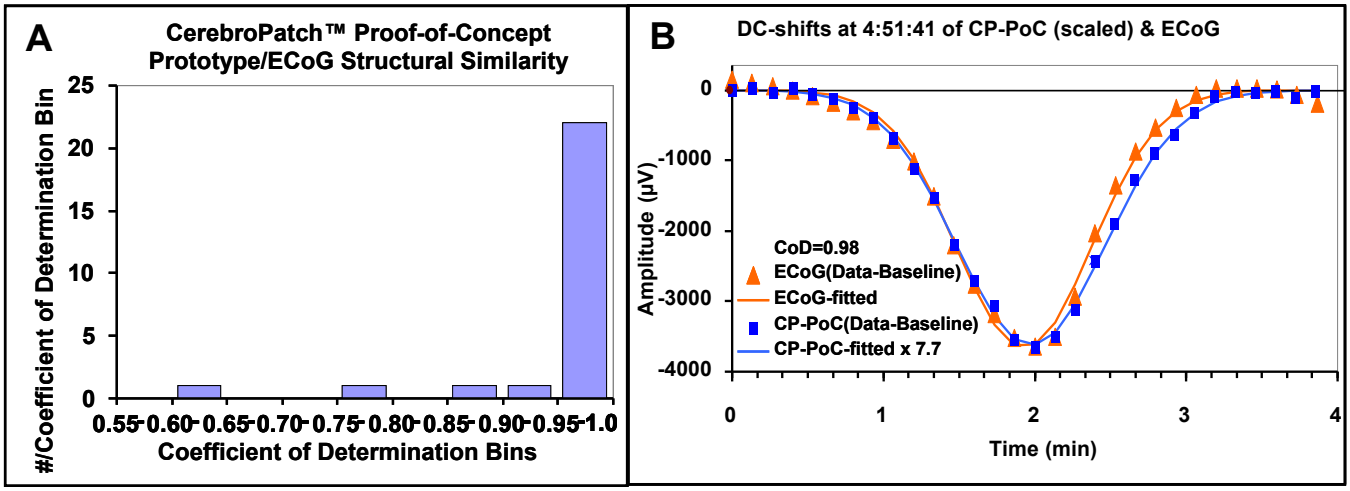

Figure 3. Panel A shows the frequency distribution of the 26 Coefficients-of-Determination (CoD) between the 8-sec data segments of ECoG strip and CerebroPatch™ Proof-of-Concept Prototype device curves showing the two excluded CoDs of 0.63 and 0.79 whose curves were deemed not similar. The remaining twenty-four DC-shift comparisons with CoDs >0.80 suggest strongly that the Prototype device detected the confirmed ECoG-coded SDs. In Panel B the 8-sec data blocks of the ECoG (red triangles) and CerebroPatch™ Proof-of-Concept (CP-PoC) Prototype (blue triangles, scaled by the 7.71 ratio of the peak signal amplitudes) signals of the largest DC-shifts are fitted to a 6 parameter baseline plus Gaussian model that show their structural similarity evidenced by a CoD of 0.98.

Supplemental Material

Supplemental Video 1

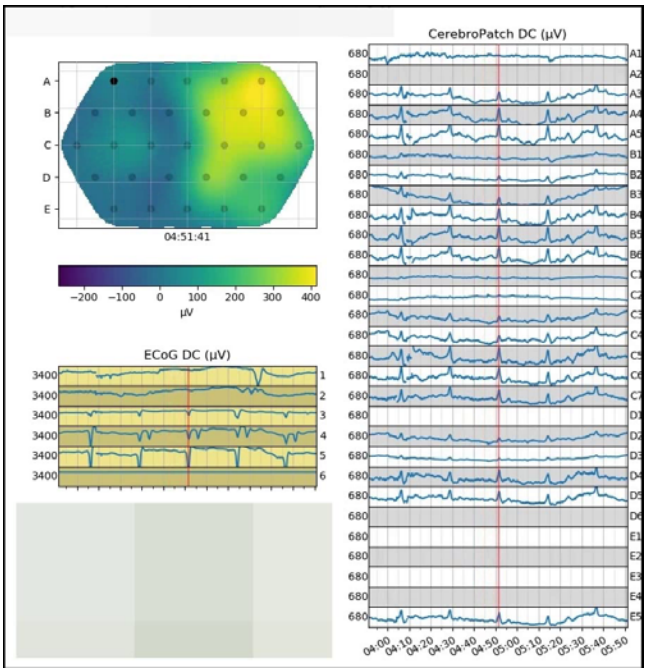

CS24-Epoch9_240722-1616.mp4

Supplemental Video 1: This video shows the reconstructed heat-map movie from the CerebroPatch™ Proof-of-Concept Prototype channel electrodes voltages for a patient with aSAH (upper left panel) with the voltage calibration pseudo-color scale from 250 to -410 µV (positive-negative reversed) just below that was depicted in Figure 2 as a still image. The extent of the scalp voltage is depicted in the heat-map movie as a “yellow” ~4 cm region of approximately -410 µV in the upper right corner of the Prototype device. The channel plots of the ECoG electrodes are shown in the lower left panel and those of the Prototype device in the right panel with the time scale below. The vertical red line is a time-marker that moves across the channel plots from 4:42:37 to 5:02:53 as shown on the time-ticker just below the movie frame created from the Prototype device data. Please note the slight DC-shift with amplitude of approximately -80 µV that rises and falls at some of the same Prototype device electrodes A5, B5, and B6 that is time-locked to the DC-shift from ECoG electrode #4 at 4:56 min:sec.